A Neon JT Cooler for Ariel

M. Hills, M. Crook, A. Eagles, G. Gilley, B. Green, S. Kendall, C. Padley, C. Pulker, T. Rawlings

STFC Rutherford Appleton Laboratory, Harwell Campus, Didcot, Oxfordshire, UK

ABSTRACT

Ariel is the fourth medium (M4) mission selected in the ESA Cosmic Vision 2015-2025 programme, with a launch planned in 2029. The spacecraft will carry two instruments: a Fine Guidance System (FGS) and the Ariel InfraRed Spectrometer (AIRS). AIRS requires active cooling of both its channels to below 42 K and this will be provided by a neon Joule-Thomson (JT) cooler developed by the Rutherford Appleton Laboratory (RAL).

This paper describes the design of the cooler to meet the requirements of the Ariel mission. We summarise the overall cooler architecture and design of the main sub-systems: the compressors, ancillary panel and JT heat exchanger assembly. Performance modelling of the compressors and heat exchangers – which permits system level trade-offs to be performed – is described. The outcomes of these trades are reported. Preliminary tests have been performed on the heat exchanger sub-assembly and these results are presented. We conclude with a summary of the current status and future developments for the flight model cooler.

INTRODUCTION

The Ariel mission will study exoplanets transiting their host star. Over the 4-year (6-year goal) mission duration, its aim is to survey around 1000 exoplanets, observing them in both the visible and infrared wavelengths to reveal the composition of their atmospheres and their thermal structure. The science payload consists of an all-aluminium off-axis Cassegrain telescope feeding two instruments: the Fine Guidance System (FGS) and the Ariel Infrared Spectrometer (AIRS). FGS incorporates three photometric channels operating between 0.5 and 1.1 μm, two of which are also used for telescope pointing, and a near-IR spectrometer working in the 1.1–1.95 μm range. AIRS is comprised of two channels (Ch0 and Ch1) that cover the 1.95–7.8 μm range, with the split occurring at approximately 3.9 μm.

The detectors selected for AIRS are Teledyne Imaging Systems' H1RGs (with HgCdTe as the photosensitive material). The standard product is suitable for Ch0, while Ch1 will require a tailored version, based on NEOCam heritage,[1] with a cut-off wavelength of 8 μm. Both versions require cooling to below 42 K in order to reduce the dark current to the necessary level and, in the case of Ch1, to maintain the long wavelength cut-off of the detector.

The Ariel spacecraft will orbit the second Lagrangian point (L2), where it will take advantage of the stable thermal environment there. The overall spacecraft thermal design is based around a warm Service Module (SVM), with body-mounted solar arrays pointing in the Sun direction, shielding a cold Payload Module (PLM), which incorporates a stack of three v-groove radiators that provide passive cooling down

Cryocoolers 21, edited by R.G. Ross, Jr., J.R. Raab and S.D. Miller

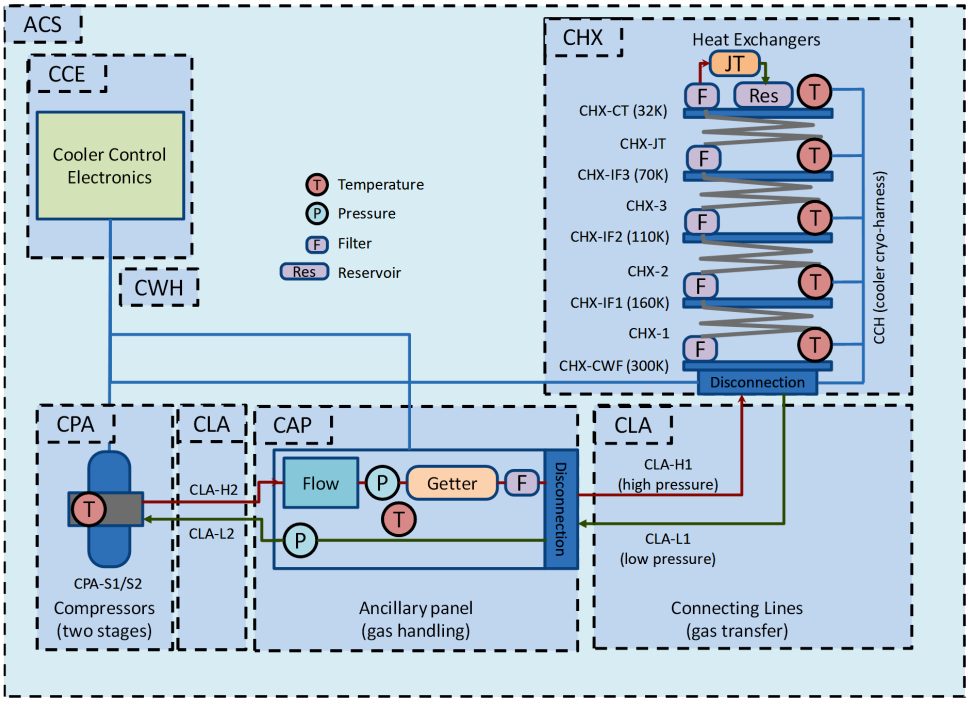

Figure 1. JT Cooler schematic

to ~ 55 K for the telescope and optical bench.[2] The additional cooling necessary to achieve < 42 K on the AIRS detectors will be provided by an Active Cooler System (ACS), which will take the form of a closed-cycle JT cooler using neon as the working fluid.

The cooler being developed at the Rutherford Appleton Laboratory to address this need builds on heritage from the 4 K JT Cooler delivered for the Planck mission, which achieved 4.5 years of continuous in-orbit operation during the successful completion of the mission.[3,4]

ARIEL COOLER REQUIREMENTS

The specific requirements for the Ariel cooler evolved throughout phase A/B1, as would be expected for this early stage of the mission development. The design presented here was targeted at providing a cooling power of 105 mW at ≤35 K with a maximum final pre-cooling temperature of 67 K (provided by v-groove 3). However, by the time of the testing reported below, this had been reduced to 88 mW at ≤35 K with a maximum final pre-cooling temperature of 60 K. In addition to the final pre-cooling temperature, the heat exchanger design must comply with the temperatures of the other available pre-cooling stages — in this case, v-groove radiators 1 and 2 — and the maximum heat that can be rejected to them. The current values for these are given later in Table 3.

COOLER CONFIGURATION

The cooler architecture is shown in Figure 1. It is typical of closed-cycle JT coolers for space, with the overall Active Cooler System split into a number of units. The Cooler Heat Exchanger (CHX) assembly contains all the cold parts of the cooler: the Cold Tip (CT) where active cooling is provided by expanding neon across a restriction, in this case an orifice; the counter-flow heat exchangers that enhance cooling performance and reduce heat rejected; and the pre-cooling interfaces, where heat is rejected at higher temperatures. A tube-in-tube architecture is chosen for the counter-flow heat exchangers, as it is simple to assemble and is significantly more effective in comparison to a side-by-side arrangement.

The one-way flow required by the CHX is generated from the Compressor Assembly (CPA): a pair of linear compressors fitted with reed valves and operating head-to-head to minimise exported vibration. Between the CPA and CHX is a Cooler Ancillary Panel (CAP) that contains instrumentation to measure the high- and low-pressure and the mass-flow rate, along with a getter for gas purity. These three units are connected with two pairs of Connecting Line Assemblies (CLAs). A Cooler Control Electronics (CCE) provides the drive for the linear compressor motors, and powers and reads out the various cooler instrumentation.

In the Ariel spacecraft, the CCE, CPA, CAP and CLAs are located in the warm SVM. The CHX is spread through the cold payload module, with the disconnection box mounted to the Payload Interface Panel (PIP), the Interfaces (IFs) mounted to the v-groove radiators and the cold tip located inside the optical bench, where it is coupled to the AIRS Ch0 and Ch1 detectors with a pair of thermal links.

NEON SPECIFIC DESIGN CONSIDERATIONS

Neon is selected as the working fluid for the Ariel cooler because its boiling point (27.05 K at 1 bar_{abs}) is well matched to the temperature requirement discussed above. Typically, the working fluid for RAL's closed-cycle JT coolers has been helium-4; the different fluid properties of neon therefore needed to be given particular consideration for this cooler. Neon has a much higher critical temperature then helium-4 (44.5 K compared to 5.2 K). Its critical pressure is also much higher than helium-4 (27.7 bar compared to 2.3 bar) and, more importantly in this case, is beyond the range typically achieved in closed-cycle JT coolers driven by linear compressors. These two facts mean that the possibility of forming liquid before the JT expansion is much greater with neon because the sub-critical region is accessible on the high-pressure side of the cooler, and this has to be considered in the design of the coldest parts of the heat exchanger.

Purity of the working gas is paramount in any JT cooler due to the small size of the JT restriction (~50 microns in this cooler). Typically, this is guaranteed through three aspects of the cooler's design and integration: firstly, a getter is fitted to the CAP to remove impurities during operation; secondly, sintered filters are employed on the heat exchanger's pre-cooling interfaces that provide a safe location for impurities with a sublimation temperature above that of the interface's temperature to freeze out; and thirdly, rigorous pump, purge and fill procedures are employed to ensure the purity of the fill gas. To minimise size, mass and power – all of which are critical for the Ariel mission – an ambient getter was selected instead of a heated version, which had been flown previously on the Planck 4 K Cooler. The compromise is that this getter cannot remove inert contaminants. Of these, nitrogen is a particular concern because at the partial pressures associated with its presence at levels below 1 ppm (which is still sufficient to block the JT orifice) it will sublime at < 43 K; this means it would not freeze out at the filter on the final pre-cooling stage, but could do so at the cold tip. There is therefore a strong emphasis on ensuring that nitrogen is removed from the fill gas to an extremely low level.

COOLER TRADE-OFF STUDIES

The generic JT cooler architecture shown in the Figure 1 may be used for a wide range of applications and must be tailored appropriately for a specific use. In the case of the heat exchangers, this involves selecting appropriate geometry to satisfy the requirements for cooling power and heat rejected to the pre-cooling interfaces. A given heat exchanger geometry will usually be able to meet the cooling power requirement for a selection of different high-pressures and mass flows – i.e. a larger high-pressure with a lower mass-flow can achieve the same cooling power as a lower high-pressure with a larger mass-flow. These parameters can then be traded off in the compressor design and at payload system level: higher high-pressures increase the compressor input power, but higher mass flows increase the heat rejected at the pre-cooling stages. Of particular concern for Ariel was to evenly distribute and, as far as possible, minimise the heat rejected to the v-grooves such that the passive cooling still provided the required temperatures on the optical bench and telescope assembly.

Sub-critical operation is targeted on the low-pressure side of the JT orifice since accumulating liquid here ensures excellent temperature stability. This means that the cold tip temperature is dictated by the saturation temperature at the low-pressure side of the orifice (note that the low-pressure produced by the compressors must be somewhat lower to account for the pressure drop in the low-pressure side of the heat exchanger).

In general, the optimisation of the cooler system is a highly iterative process involving compressor, heat exchanger and system level considerations.

HEAT EXCHANGER DESIGN AND OPTIMISATION

Mechanical Design

The heat exchanger mechanical design and manufacture are based on heritage from the Planck 4 K Cooler. The heat exchanger tubes are stainless steel, vacuum brazed into copper manifolds that route the high-pressure pipe inside the low-pressure pipe. The copper manifolds are soldered to blocks containing the filters, which provide the thermal connection with pre-cooling interfaces.

The cold tip incorporates the JT orifice and a porous sinter to retain liquid produced on the outlet side of the orifice. The sinter is assembled into a copper block and the thermal links to the AIRS detectors are connected to this. The orifice consists of a laser drilled hole in a domed pipe end. This pipe end is physically separated from the copper block by the length of the inlet pipe and is joined to the outlet pipe in a copper ferrule; these pipes provide a degree of thermal isolation that allows the orifice to be heated, using a resistor attached to the copper ferrule, without raising the temperature of the cold tip thermal interface. This feature is useful in case the orifice should need to be warmed to release frozen-out impurities that would cause a reduction in mass-flow, or, in the worst case, a blockage.

Model Description

The neon JT cooler heat exchangers have been designed using a thermodynamic model developed at RAL. Rather than using analytical solutions for the heat exchanger effectiveness based on the NTU method,[5] the model divides each section of heat exchanger into a series of cells. Each of these cells contains a sub-cell for the warm gas, cold gas and the outer pipe wall. Energy balances are performed for each sub-cell to determine their temperatures. Since the thermophysical properties that determine the heat transfer between cells are themselves functions of temperature, the calculations must be performed iteratively. An initial estimate of the temperature profile in the heat exchanger (based on a linear function) is made to start the calculation and the model iterates until the temperature difference between successive iterations falls below the set convergence criterion. Once the cell temperatures are known, heat exchanger effectivenesses, heat rejected and cooling power can be computed. The thermophysical properties of neon used in the calculations were obtained from REFPROP version 9.1.[6]

Initial Trade-offs

Initially, three operating temperatures were considered: 30 K (low-pressure = 2.23 bar), 32 K (low-pressure = 3.54 bar) and 34 K (low-pressure = 5.34 bar). A higher low-pressure means that higher high-pressures can be accessed with the same compression ratio and this increases the cooling power. However, this puts more demands on the compressors in that they need to be designed to operate further from typical operating pressures of previous RAL designs and, more importantly, the electrical input power required goes up. A nominal cold tip temperature of 32 K was targeted as a compromise between these factors. and, more importantly, the electrical input power required goes up. A nominal cold tip temperature of 32 K was targeted as a compromise between these factors.

To maximise cooling power, it is desirable to reduce the temperature of the final pre-cooling stage as far as possible and from this it follows that v-groove 3 should always be used as a pre-cooling stage. Heat rejection considerations drive the selection of the other pre-cooling stages. Achieving a high effectiveness heat exchanger – and thereby reducing the heat rejected on the pre-cooling stage – becomes increasingly challenging as the temperature difference bridged by the heat exchanger gets larger. Given that the largest temperature difference in the Ariel v-grooves occurs between the PIP and v-groove 1, it natural to make use of this v-groove as a pre-cooler. In order to spread the heat rejected by the cooler further and to reduce the load on v-groove 3, it was decided to also make use of the v-groove 2 for the detailed heat exchanger optimisation. This decision was a trade-off with the increased mechanical and integration complexity from using all three v-grooves, but this drawback was judged to be worth the benefit from improved system level thermal performance.

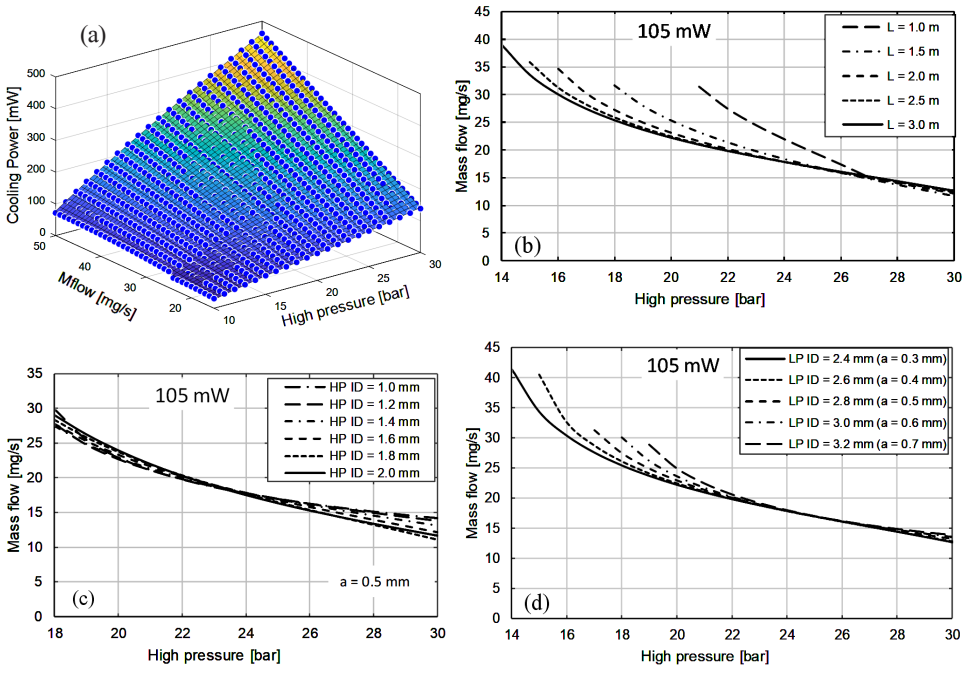

Figure 2. (a) example plot of cooling power as a function of high-pressure and mass flow for a given JT heat exchanger geometry; the points show the model results, the surface shows the fit function; (b) lines of constant cooling power (105 mW) on axes of high-pressure and mass flow for different JT heat exchanger lengths and fixed pipe diameters; (c) lines of constant cooling power (105 mW) on axes of high-pressure and mass-flow for different JT heat exchanger high-pressure pipe diameters with constant annular gap (a = 0.5 mm) for low pressure flow, heat exchanger length is fixed; (d)) lines of constant cooling power (105 mW) on axes of high-pressure and mass-flow for different annular gaps in the JT heat exchanger, high-pressure pipe diameter (inner diameter = 1.4 mm, outer diameter = 1.8 mm) and heat exchanger length are fixed.

Optimisation

For given cold tip and pre-cooling temperatures, the JT cooling power is determined by the high-pressure, mass-flow and the effectiveness of the JT heat exchanger (CHX-JT). Heat exchanger optimisation is concerned with maximising effectiveness by tailoring the geometry, and this process is illustrated by the plots in Figure 2. The model is used to predict the cooling power over a range of high-pressures and mass-flow for a given heat exchanger geometry. A surface fit is applied to these data (Figure 2(a)) and the resulting function is used to plot lines of constant cooling power (105 mW in this case) that meet the requirement on axes of mass-flow and high-pressure. These lines define the trade-off between mass-flow and high-pressure for a given heat exchanger geometry. As can be seen from the Figure 2(b), increasing the heat exchanger length can achieve the cooling power requirement at lower mass flows for a given high-pressure. However, beyond a length of 2.5 m, the gains become small in this case.

The bottom two plots in Figure 2 show the effect of changing pipe diameter. Figure 2(c) illustrates that changing the diameter of the high-pressure pipe has minimal impact on the heat exchanger performance: lines of constant cooling power for diameters from 1 mm to 2 mm lie on top of each other. However, as shown in Figure 2(d), the performance is improved if the diameter of the low-pressure pipe is reduced, while keeping the high-pressure pipe diameter constant. The result of this is that, for a given high-pressure, lower mass flows are needed to achieve the same cooling power. The reason for the performance improvement is that the reduction in diameter of the low-pressure pipe causes a reduction in annular gap for the low-pressure flow and, with it, the hydraulic diameter (d_h); this acts to increase the heat transfer

Table 1. Selected heat exchanger geometry

Heat exchanger	High pressure tube ID (mm)	High pressure tube OD (mm)	Low pressure tube ID (mm)	Low pressure tube OD (mm)	Length (mm)
HX1	1.37	1.83	2.8	3.5	2000
HX2	1.37	1.83	2.8	3.5	1500
HX3	1.37	1.83	2.8	3.5	1500
HXJT	1.2	1.9	2.72	3.28	2500

coefficient (h) between the low pressure flow and the outer wall of the high pressure pipe for a given thermal conductivity (k) and Nusselt number (Nu):

$$h = \frac{Nu.k}{d_h} \quad (1)$$

The penalty for reducing the annular gap is, of course, an increase in pressure drop. However, for the relatively high pressures in the low-pressure line of this JT cooler, this is not a strong design driver. Furthermore, the 32 K operating point gives good temperature margin, so a small rise in the low pressure at the cold tip is not critical. Ultimately, practical manufacturing and assembly constraints set the limit on how far this reduction of the low-pressure flow channel can be taken. The geometry that was eventually selected for all heat exchangers is detailed in Table 1.

COMPRESSOR OPTIMISATION

A compressor swept rate to match different heat exchanger operating cases (i.e. high-pressure and mass-flow) can be defined in terms of piston size, stroke and operating frequency. These parameters are optimised to meet resonance conditions for each compression stage in order to determine the best compressor configuration, and hence size and input power for each case. Compressor performance modelling was undertaken to identify these parameters using models developed at RAL[4] and validated against existing compressors operating with neon gas. The outcome is summarised in Table 2, which targets the nominal operating point for the cooler: high-pressure = 20 bar_{abs}, low-pressure = 3.5 bar_{abs} and mass-flow = 20 mg/s. It should be noted that the ACS is required to meet performance at ± 5 Hz from its nominal frequency of 48 Hz and the worst case input powers must be calculated at the extreme running frequencies (i.e. 43 Hz and 53 Hz).

TEST RESULTS

To confirm the heat exchanger performance and validate modelling, a demonstrator model of the CHX was tested in an open loop configuration with neon flowing from a bottle into the high-pressure line. The low pressure was regulated at ~3.5 bar using a control valve on the heat exchanger outlet. The cryogenic test hardware is shown in Figure 3. A commercial Gifford-McMahon (GM) cryocooler was used to simulate the pre-cooling that would be provided by the Ariel v-grooves. All heat exchangers were contained within the outer radiation shield (not shown) except HX1, which is coiled in a room temperature radiation environment.

Table 2. Summary compressor design parameters

Compressor parameter	Stroke amplitude (mm)	Freq (Hz)	Spring rate (N/mm)	P high (bar_{abs})	P low (bar_{abs})	Mass flow (mg/s)	Compressor input power (W)
Nominal value	5.4 (72%)	48	18	20	3.5	20	33

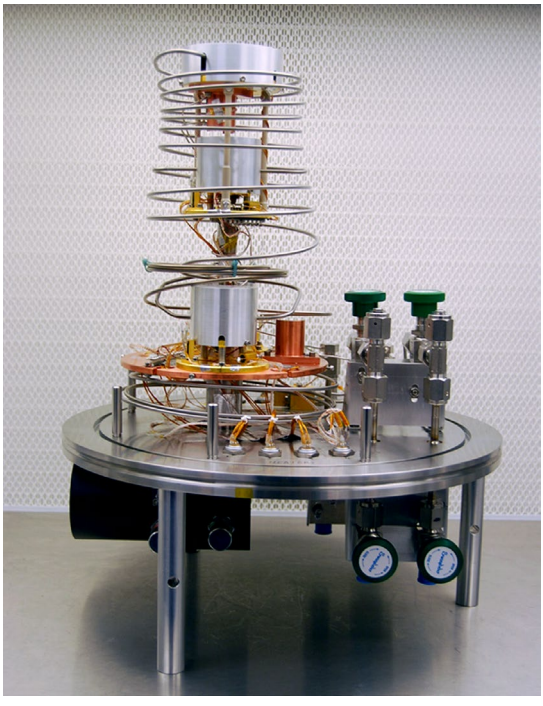

Figure 3. CHX test assembly

In addition to confirming temperature and cooling power, a key objective of the test campaign was to measure the heat rejected by the cooler at the pre-cooling interfaces. This was achieved using thermal shunts, which created a thermal break between the heat exchanger interfaces and the copper plates attached to the commercial cryocooler. They also featured PID (Proportional Integral Derivative) controlled heaters on the side of the shunts to which the cooler interfaces were mounted; this kept the rejection temperature at a constant known value. The shunts were calibrated prior to the test so that the total heat flow across them could be inferred from the temperature difference between the top and bottom surfaces; the PID heater power was then subtracted from the total to obtain the heat rejected by the cooler.

A GSE ancillary panel was used to measure the high-pressure flow, the low-pressure return and the mass-flow. The mass-flow meter was placed in the return line from the CHX. Both pressure and mass-flow sensors were COTS (Commercial Off-The-Shelf) items.

Prior to entering the CHX assembly, the neon gas from the bottle was passed through two cold traps. The first was a simple liquid nitrogen trap which was kept topped up with liquid throughout the test. The second consisted of a series of filters thermally linked to the first stage of a commercial GM machine, which was housed in its own dedicated cryostat. PID controlled heaters on the first stage of the GM were used to maintain the filters at the required temperature; typically, this was as cold as possible without risking liquefying neon in the line (for the high-pressures used this meant between 38 and 43 K). The purpose of this "trap cryostat" was to remove any impurities that would not freeze out in the filters at the CHX pre-cooling stages – as discussed above nitrogen was the main concern. A total test time of nearly two weeks was accumulated without any blocking of the orifice, indicating that this approach is an effective method for achieving the necessary purity in the working gas.

A summary of the cooling power measurements is given in Table 3. In addition to the heat load applied to the cold tip, there was a continual parasitic radiation load from the outer radiation shield. The shield temperature was used to calculate this load and the result of including it in the total cooling power is shown in the next-to-last row of Table 3.

The Ariel cooling power requirement was comfortably met at the maximum v-groove temperatures, with a high-pressure of 19.9 bar and mass-flow of 23.8 mg/s (measurement #2), and is also with a high-pressure of 17.9 bar and a mass-flow of 21.9 mg/s (measurement #3). These operating conditions are

Table 3. Heat exchanger performance summary

Parameter	Requirement	Measurement #1	Measurement #2	Measurement #3
High pressure (bar_{abs})	20	19.94	19.90	17.91
Low pressure (bar_{abs})	3.54	3.58	3.55	3.53
Mass flow (mg/s)	20	23.91	23.80	21.86
IF1 temperature (K)	115-150	160.22	150.19	150.20
IF2 temperature (K)	75-100	107.15	100.15	100.15
IF3 temperature (K)	45-60	66.92	60.03	60.03
CT temperature (K)	< 35	32.70	32.89	32.77
Heat rejected at IF1 (mW)	65-180	230.49	253.36	227.08
Heat rejected at IF2 (mW)	20-120	59.78	52.09	43.65
Heat rejected at IF3 (mW)	40-140	116.83	140.22	113.28
Heat applied at CT (mW)	N/A	81.01	122.13	88.06
Cooling power including parasitics (mW)	> 88	94.29	133.51	99.33
Predicted heat lift at CT (mW)	N/A	106.5	146.4	110.8

expected to be comfortably within the capability of the Ariel compressors, which are designed to deliver the values given in the Requirement column of Table 3. Measurement #1 shows the cooling power that could also be achieved with the v-grooves at the maximum temperatures from the initial phase of the Ariel payload study.

The heat rejected to the pre-cooling stages was within requirements for all cases except IF1. The higher load here was attributed to additional parasitic loads present in the test bench, which would not occur in the payload configuration.

The correlated heat exchanger model gives agreement with the measured cooling power to within ~10 %. Some of this error may be due to the error involved in estimating the parasitic radiative load on the cold tip. In any case, this level of agreement, in combination with the payload thermal margins philosophy, is sufficient to support the design trade-offs at system level in the coming phase of the project. The projected performance for a high-pressure of 20 bar and a mass-flow of 24 mg/s is summarised in Figure 4, with the cooling power from measurements #1 and #2 plotted for comparison. Available cooling power increases rapidly as the v-groove 3 temperature drops, but so does the load on that v-groove 3. The latter effect can be managed by reducing mass-flow since the cooling power exceeds the current requirement at

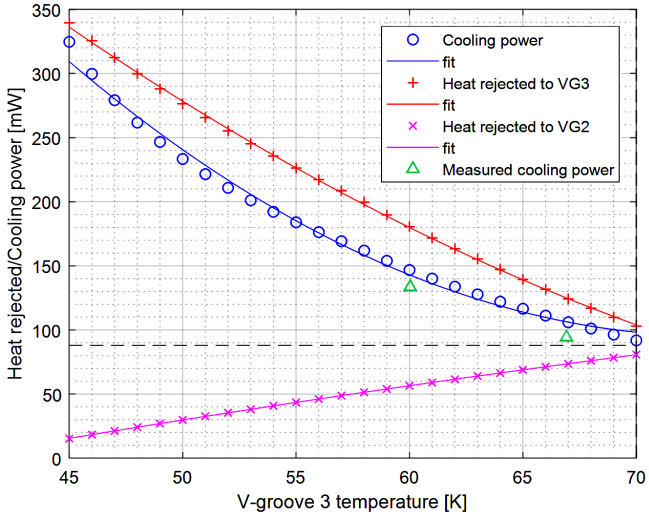

Figure 4. Modelled JT cooler performance for Ariel as a function of v-groove 3 temperature. The dashed line illustrates the cooling power requirement (88 mW).

any v-groove 3 temperature below 70 K. The final cooler operating point will depend on the temperature of all v-grooves in the Ariel payload.

CONCLUSIONS AND FURTHER WORK

A neon JT cooler has been designed and optimised to meet the requirements of the Ariel mission. A demonstrator model of the cooler heat exchanger assembly has been built and tested in an open loop configuration. The results have successfully demonstrated the cooling power needed for Ariel. The next steps are to perform full cooler system level tests in closed loop with the JT compressors and this activity will start in 2021.

ACKNOWLEDGMENT

This work was funded by UK Research & Innovation's Science & Technology Facilities Council, the European Space Agency (under contracts 4000119824/17/NL/IB and 4000121153/18/NL/HB) and the UK Space Agency. The authors gratefully acknowledge support from Thierry Tirolien and Mortiz Branco at ESA.

REFERENCES

1. McMurty, C. *et al.*, "Development of sensitive long-wave infrared detector arrays for passively cooled space missions," *Optical Engineering*, vol. 52, no. 9 (2013), p. 091804
2. Morgante, G. *et al.*, "The thermal architecture of the ESA ARIEL payload at the end of Phase B1," *Experimental Astronomy* (in press)
3. Planck Collaboration, "Planck early results. II. The thermal performance of Planck," *Astronomy & Astrophysics* 536 (2011), A2.
4. Crook, M. *et al.*, "Development of a 2K Joule-Thomson Closed-Cycle Cryocooler," *Cryocoolers 19*, ICC Press, Boulder, Colorado (2016), pp. 9–18.
5. Eastop, T.D. & McConkey, A., *Applied Thermodynamcs for Engineering Technologists*, 5th ed., Longman, Singapore (1998), pp 623–627
6. Lemmon, E. W., Huber, M. L., McLinden, M. O., *NIST Standard Reference Database 23: Reference Fluid Thermodynamic and Transport Properties-REFPROP*, Version 9.1, NIST (2013).